HAL
open science

Selective elimination of phenol from hydrocarbons by zeolites and silica-based adsorbents-Impact of the textural and acidic properties

Ibrahim Khalil, Karine Thomas, Hicham Jabraoui, Philippe Bazin, Françoise Maugé

To cite this version:

Ibrahim Khalil, Karine Thomas, Hicham Jabraoui, Philippe Bazin, Françoise Maugé. Selective elimination of phenol from hydrocarbons by zeolites and silica-based adsorbents-Impact of the textural and acidic properties. Journal of Hazardous Materials, 2020, 384, pp.121397. 10.1016/j.jhazmat.2019.121397 . hal-02345827

HAL Id: hal-02345827

https://hal.science/hal-02345827v1

Submitted on 17 Dec 2020

HAL is a multi-disciplinary open access archive for the deposit and dissemination of scientific research documents, whether they are published or not. The documents may come from teaching and research institutions in France or abroad, or from public or private research centers.

L'archive ouverte pluridisciplinaire **HAL**, est destinée au dépôt et à la diffusion de documents scientifiques de niveau recherche, publiés ou non, émanant des établissements d'enseignement et de recherche français ou étrangers, des laboratoires publics ou privés.

Selective elimination of phenol from hydrocarbons by zeolites and silica-based adsorbents – Impact of the textural and acidic properties

Ibrahim Khalil[1], Karine Thomas[1*], Hicham Jabraoui[2], Philippe Bazin[1], Francoise Maugé[1]

[1] Laboratoire Catalyse et Spectrochimie, ENSICAEN, Université de Caen Normandie, CNRS, 6, bd du Maréchal Juin, 14050 Caen, France

[2] Laboratoire Physique et Chimie Théoriques (LPCT) UMR 7019 CNRS, Université de Lorraine, F-54000 Nancy, France

* corresponding author: karine.thomas@ensicaen.fr

Keywords: Phenol adsorption; Toluene adsorption; Selectivity; Zeolite acidity; Breakthrough curves;

Highlights:

- Phenol condensed in Y zeolite supercages but adsorbed on external silanol groups
- HY selectively adsorbed phenol in presence of toluene and linear hydrocarbon
- Easy regeneration requires low amount of acidic sites

ABSTRACT

This paper investigates the parameters that influence the selective adsorption of phenol, toxic molecule, from a semi-model biofuel mixture containing alkanes and different proportions of aromatic compounds. The adsorption capacity, selectivity and regeneration ability of different adsorbents, i.e. zeolites, silica-based solids, alumina and activated carbon, were related to their textural properties and to the nature, strength or location of their acidic sites. This work demonstrates that phenol differently adsorbs in the micropores and mesopores. In the micropores of faujasites, phenol is condensed into the supercages. Otherwise, in the mesopores of the zeolite, phenol interacts with the silanol groups. On purely siliceous adsorbents, a ratio of one phenol adsorbed on one silanol group could be established. As for selectivity, the strong acidic sites of the faujasites are necessary to favor phenol adsorption compared to toluene one. By contrast, the amount of strong Brønsted and Lewis acid sites limits regeneration. Hence, a compromise has to be found and the best performances were obtained using a slightly dealuminated zeolitic adsorbent presenting both micro and mesopores.

1. INTRODUCTION

Global energy demand is expected to grow by around the third between 2018 and 2040 [1], resulting an increase in the fossil fuel consumption known as the most common source of energy on our planet [2]. However, the serious environmental changes (global warming), caused by the CO_2 emissions produced after burning the fossil fuels in vehicles, restrict their excessive use in the next years [3–5]. For such a purpose, governments around the world has raised concerns and increased the focus on the research for the development of environmentally friendly renewable sources of fuel and energy [6].

New generations of transportation biofuels have recently been introduced, involving a partial or complete replacement of fossil fuels by renewable resources as those derived from biomass [7]. Biofuels of first generation are produced from food and agriculture [3]. They are currently used in many countries as pure fuel source (e.g. bioethanol) or in mixtures with fossil fuels (e.g. biodiesel) [8]. They contribute in the reduction of green-house-gas emissions but they create a negative impact on food security [9]. Nowadays, a significant effort is deployed on processing second generation biofuel production i.e. that is issued from non-edible biomass [3], as lignocellulosic biomass from wood and agricultural wastes [10]. Oils obtained from the pyrolysis of this biomass present similar physicochemical and rheological properties to crude oils [4]. However, their high viscosity, corrosiveness and low energetic power related to their high oxygen content (20 - 55 wt.%) limit their uses [2,11]. Therefore to obtain bio-oils compatible with the crude oil feedstock, oxygen should be removed [12,13]. In this way, pyrolytic bio-oils can be upgraded by a first hydrodeoxygenation (HDO) step. The upgraded bio-oils are further co-proceeded with a vacuum gas oil (VGO) in a fluid cracking catalytic (FCC) unit [14]. Due to the hydrogen transfer occurring during FCC process, the cracking products contain a lower amount of oxygen (0.5 wt.% to 7 wt.%), mainly composed of substituted phenol type molecules [7,8]. However, phenolic compounds are highly toxic compounds for health. Nabi et al. [3] have studied the effect of these phenolic impurities on the combustion efficiency of the biofuels. Their results have shown a decrease in the motor efficiency followed by the production of toxic exhaust gases (NO and non-burned hydrocarbons) after the biofuels combustion step [3]. Such reasons recommend the elimination of these phenol-type impurities to obtain ultra-pure bio-fuel. In

this work, we investigate a purification process based on the selective adsorption of phenolic impurities in a semi-model biofuel mixture, using well-selected porous materials, with different properties (porosity, acidity: type, amount and strength…), as adsorbents.

Adsorption is a well-known separation process [15]. It allows a selective capture of the undesired product that can be further valorized, after a desorption step, for other applications. The adsorbents must combine both high adsorption capacity and selectivity toward the molecules to eliminate [16]. In addition, adsorbents regeneration under mild conditions is an important property that allows the reuse of the adsorbents in several adsorption cycles [16–19]. Most of the studies dealing with the selective adsorption of phenol and its derivates were reported in aqueous solutions, in particular from wastewater [16–18,20,21], since phenol and its derivates are considered as priority pollutants even at low concentration [22–26]. Roostaei et al. [27] studied the adsorption of phenol from water (2.2 mmol/L – 0.02 wt.%) using Y zeolites. During the adsorption, the equilibrium state was quickly reached (0.27 mmol/g), and a reversible adsorption was obtained, after a regeneration step at 360°C under air atmosphere for 16 hours [27]. For the same purpose, Khalid et al. [17] used Y zeolites, with different Al loading (5 < Si/Al < 100), as adsorbents. They show that the high aluminum content in the zeolite framework decreases the selectivity toward phenol molecules, due to the high affinity of aluminum atoms for water molecules. At an initial phenol concentration of 17.4 mmol/L, the amount of adsorbed phenol decreased from 50.5 mmol/g to 13 mmol/g when the Si/Al ratio decreases from 100 to 5, respectively [17]. The authors reported that, for an adsorption capacity of 50.5 mmol/g, phenol molecules occupy only 20% of the micropore volume of the zeolite (0.285 cm^3/g). The residual pore volume in the zeolite was or inaccessible or filled by co-adsorbed water molecules that compete phenol adsorption [17]. For both studies a comparison of the efficiency of zeolites adsorbents with activated carbon, points out the highest adsorption capacity of this last adsorbent, especially for high phenol concentration (> 13 mmol/L) [17,27]. However, its high regeneration cost, in comparison to other adsorbents such as zeolites, limits its use for industrial realm [28–30].

On the other hand, only few studies dealt with the elimination of phenol derivates from hydrocarbons. Two patents published in 1952 [31] and 1971 [32], studied respectively the phenol removing by treating with a strong alkali metal hydroxide solution [31], and the phenol adsorption over polyurethane foams followed by regeneration in acetone [32]. From that time, environmental standards have widely changed, and these two processes remain far from the requirement of green chemistry. In a previous work [33], we have studied the adsorption of phenol from isooctane and 1 wt.% n-nonane using protonated HY zeolites with different Si/Al ratios (from 2.5 to 40). The composition of the mixture was chosen in a way to allow studying the adsorption capacity of the zeolites towards phenol in absence of any competitional adsorbates. Phenol was adsorbed in both supercages and mesoporous of the zeolites. Filling the supercage was conducted by the configuration of adsorbed phenol molecules, whatever the Al loading, 3 phenol molecules were adsorbed in each supercage (≈ 55% of the micropore volume). However, the parameters affecting the phenol adsorption in the mesoporous of the zeolite were not investigated. Solids regeneration was shown to be limited by the number of the total Brønsted (BAS) and Lewis (LAS) acid sites, and the quantification of the acid sites draws us to conclude that one phenol molecule remains over each acid site [33]. In another work, DFT calculations were used to calculate the interaction energies of phenol over BAS and LAS of HY zeolite (Si/Al = 47), and results confirm the low regeneration observed over high aluminum loaded zeolites ($E_{phenol\text{-}BAS}$ = -79 kJ/mol and $E_{phenol\text{-}LAS}$ = -199 kJ/mol) [34]. Moreover, we showed the presence of two interaction modes of phenol with the surface of the adsorbents: the first *via* its oxygen atom, while the second corresponds to an interaction *via* its aromatic ring [34]. So far, the effect of the presence of aromatic compounds, that corresponds to 30 – 50 vol.% of the 2nd generation biofuels fraction, was not studied for phenol selective adsorption from biofuels. Regarding the used adsorbents, aromatic compounds can widely affect the selectivity toward phenol adsorption, especially when weak interactions take place or when phenol molecules are adsorbed *via* their aromatic ring. The aim of this paper is to study the phenol selective adsorption for 2nd generation biofuels purification over low cost materials with different textural properties and acidic strength. An understanding of the parameters that influence the adsorption capacity of various adsorbent materials will be investigated. Moreover, the effect of the

strength of the OH groups on the selectivity toward phenol adsorption in presence of different concentrations of aromatic compound (toluene) will be tackled to identify the parameters that can inhibit the selective biofuels purification.

In this context, we propose adsorption process to study the selective removal of phenol from a hydrocarbon mixture using a series of different solid adsorbents. Their performances are assessed in term of the adsorption capacity, selectivity and ease of regeneration of the materials by measurements with different mixtures containing phenol, n-nonane, isooctane and various amount of toluene (model aromatic compound). Protonated Y zeolites with different Si/Al ratios (from 2.5 to 40) were firstly selected to well understand the influence of the Si/Al ratio and the textural properties on the adsorption capacity in batch and flow reactors. Secondly, the influence of the zeolitic structure was assessed by comparing the performances of HY zeolites to that of ZSM-5 zeolite. Moreover, weak acid silica-based solids (mesoporous and amorphous silica) and alumina were added to the series of tested materials, and finally, the activities of all the adsorbents were compared to activated carbon, known as a reference adsorbent.

2. EXPERIMENTAL PART

2.1 Adsorbents

NH_4^+Y zeolites with Si/Al ratio of 2.5 and 2.9 were supplied by Union Carbide. Ultra-stable HY (USY) zeolites with various Si/Al ratios (22, 33, and 40) as well as proton exchanged ZSM-5 zeolite (Si/Al = 42) were supplied by Zeolyst International. MCM-41 was prepared following the procedure of Grün et al. [35]. Amorphous silica (Aerosil 200 from Degussa, called SiO_2 in the text), known as a volatile material due to it very low density, was mixed with water (120% of its total pore volume) and then calcined at 673 K to facilitate its use. The γ–alumina and the amorphous silica-alumina (called ASA in the text - 99.1 wt.% SiO_2, 0.9 wt.% Al_2O_3) solids were supplied respectively by Sasol and Grace Davison. The activated carbon (called AC in the text), used as a reference adsorbent, was provided by Norit.

2.2 Characterization techniques

The chemical composition of the zeolites was checked by inductively coupled plasma (ICP) optical emission spectroscopy using a Varian ICP-OES 720-ES. Their textural properties were characterized by nitrogen adsorption isotherms at 77K using gas adsorption system ASAP 2020 (Micrometrics) for a relative pressure (P/P_0) varying between 0.05 and 1. Total and external surface areas were determined using the Langmuir isotherms for the zeolites samples and α-plot method for the MCM-41 silica, with LiChrospher Si-1000 Silica (surface area of 26.2 m^2/g) as a reference [36]. Over the zeolite samples, the external surface represents the surface of the outside of the zeolite grains as well as that of the pores larger than micropores (>1.3 nm). For all the samples except zeolites, BET adsorption method was applied to calculate the pore volume and the surface area.

The quantification of hydroxyl groups and acidic sites was performed using infrared (IR) spectroscopy. Each sample was pressed, under a pressure of 10^7 Pa, into a precisely weighted self-supported wafer (10 - 15mg) with a surface of 2 cm^2. Prior to any experiment, sample wafer was pre-treated *in-situ* in the IR cell by heating from 298K to 623K (1 K/min) followed by an isotherm at 623K for 4 hours under secondary vacuum (10^{-4} Pa). The FTIR spectrometer used was a Thermo Fischer 6700 equipped with a MCT detector. 64 scans were accumulated for each measurement with a resolution of 4 cm^{-1}. Note that the graphical resolution is greater than the spectral resolution and is close to 0.5 cm^{-1}. The spectra displayed correspond to the difference between the spectrum after adsorption (or desorption) and the spectrum corresponding to the activated (pre-treated) sample. All spectra were normalized to a constant disc mass (5 mg/cm^2 of dried catalyst). To quantify the different OH groups of the zeolites and the silica-based samples, four IR bands were taken into consideration : (1) the ν(OH) band at ~3645 cm^{-1} that refers to zeolitic supercage OH groups of Y zeolites, that presents a molar absorption coefficient of $\varepsilon(\nu_{OH\ supercage})$ = 7.5 cm/µmol, (2) the ν(OH) band at ~3550 cm^{-1} related to zeolitic sodalite cage OH groups of Y zeolites, the molar absorption coefficient of this band is $\varepsilon(\nu_{OH\ sodalite\ cage})$ = 5.6 cm/µmol [37], (3) the ν(OH) band at ~3615 cm^{-1} characteristic of the framework OH groups of the ZSM-5 zeolite (molar absorption coefficient of $\varepsilon(\nu_{OH\ ZSM\text{-}5})$ = 3.5

cm/µmol [38], finally, (4) the combination band (ν+δ)OH located at around 4600 cm^{-1} that refers to silanol groups. Note that for silanol group, the quantification based on the area of the combination band at 4600 cm^{-1} is preferred to that of the fundamental ν(OH) at ~3740 cm^{-1}. Indeed, the molar absorption coefficient of this latter, $\varepsilon(\nu_{Si\text{-}OH})$, strongly depends on H-bonding interactions [39], making the area of the whole ν(SiOH) massif not proportional to the Si-OH concentration. By contrast, it is possible to accurately calculate the amount of silanol groups using the sharp (ν+δ)OH combination band located at about 4600 cm^{-1} with the molar extinction coefficient determined by Gallas *et al.*, $\varepsilon_{(\nu+\delta)OH}$ = 0.16 cm/µmol [39].

For acid sites characterization, pyridine was used as probe molecule. After pretreating the solid wafer in the IR cell, pyridine vapor was introduced at RT with calibrated doses from 0.05 to 1.70 µmol. A final equilibrium pressure of 266 Pa was further established in the IR cell. Finally, thermal desorption was carried out under secondary vacuum step by step from RT up to 423K for 20 minutes at each temperature. Acidic sites of the solids were quantified from the IR spectra of the pyridine adsorbed (Figure SI-1). The amount of Brønsted acid sites was determined by integrating the area of the characteristic band v8a of the pyridinium ions (PyH^+) at 1545 cm^{-1} and using its corresponding molar absorption coefficient: $\varepsilon(PyH^+)$ = 1.8 cm/µmol [37]. The amount of strong Lewis acid sites was calculated using the molar absorption coefficient, ε(PyL) = 1.5 cm/µmol, of the band v19b at ~1445 cm^{-1} characteristic of the coordinated pyridine species (PyL) [37].

2.3 Adsorption experiments

Adsorption experiments were performed either in batch or in flow conditions. Phenol purchased from Aldrich (99.5% purity) was used as a model molecule on all the adsorption studies. The liquid solution containing phenol was obtained by dissolving 7.0 g (1 wt.%) of phenol into 1000 ml isooctane (Aldrich 99+% purity). 1 wt.% of n-nonane (Aldrich 99.9% purity) was added as internal standard. Further, the selective adsorption of phenol was studied by adding, to the previous mixture, various concentrations of toluene (1, 10 and 40 wt.%) in a way to keep the same mass percent of phenol and n-nonane (1 wt.%) in the whole mixture. For both batch and flow experiments, solids were pretreated *in-*

situ at 623K for 4 hours under argon flow before performing the adsorption experiments at room temperature (25°C) and under atmospheric pressure. This activation allows the elimination of physisorbed water as well as obtaining the acidic form of the zeolites i.e. H^+Y from NH_4^+Y zeolites.

For batch experiments, a specific system was developed allowing *in-situ* activation and transfer of the powder into the hydrocarbon mixture under inert gas before the adsorption measurements (Figure SI-2). In batch conditions, 0.3 g of solid, with a particle size ranging between 200 and 400 µm, were poured into a two-neck round bottom flask (50 mL) containing 20 ml of the hydrocarbon mixture. The flow adsorption tests were performed in a glass column (300 mm of high and 6 mm of internal diameter). 0.5 g of adsorbent, with a particle size between 200 and 400 µm, were packed giving a bed volume surging from 2 to 3 cm^3. After the *in-situ* pretreatment stage, the solution to purify was fed into the column using a Gilson pump allowing a constant flow rate of 1 ml/min. For batch and flow systems, solution was collected periodically and analyzed using a Shimadzu 2010 gas chromatograph equipped by a CP-sil 5CB capillary column (30 m), using a flame ionization detector and nitrogen as carrier gas. Results of flow adsorption experiments were obtained as a breakthrough curve and the amount of phenol adsorbed per gram of solid was calculated using the following formula (F_1):

$$(F_1) \qquad q = \frac{C_0.D.t_R}{m_{ads}}$$

where q is the amount of adsorbed phenol by gram of solid (mmol/g), C_0 is the initial phenol concentration (mmol/L), D is the flow rate of the charge containing phenol (L/min), t_R corresponds to the retention time (min) when the ratio of C_t/C_0 is equal to 0.5, and m_{ads} is the mass of the adsorbent (g). The capacity of the most promising adsorbents to perform several runs was tested on additional adsorption cycles performed after a thermal desorption at 473 K for 4 hours under Argon flow (90 ml/min).

3. RESULTS AND DISCUSSION

3.1 Adsorbents characterization

3.1.1 Textural properties

Table 1 gathers chemical and textural properties of the studied solids. N_2 adsorption isotherms are presented in Figure SI-3. HY2.5 zeolite presents high surface area and high microporous volume. The low external surface area and the negligible mesoporous volume is consistent with the quasi-absence of defects in the zeolite structure. HY2.9 zeolite was obtained after dealuminating the parent HY2.5 zeolite without performing any acid washing, which explain its lower surface area, its slightly higher external surface as well as the presence of some mesoporous volume in its structure, in comparison to the parent HY2.5 zeolite. The greater Si/Al ratio of the USY zeolites (dealuminated zeolites) is associated with the creation of mesopores (up to ~0.20 cm^3/g) that increase the external surface area. The ZSM-5 zeolite presents a total pore volume of 0.28 cm^3/g, formed by both microporous (0.15 cm^3/g) and mesoporous (0.13 cm^3/g). The surface areas of the non-zeolitic metal oxides, i.e. SiO_2, ASA, alumina and MCM-41, range from 203 to 984 m^2/g. These non-zeolitic materials do not present any micropores. By contrast, activated carbon presents a high surface area (1076 m^2/g) and a pore volume almost exclusively formed by micropores.

Table 1 - Chemical and textural properties of the studied adsorbents.

Adsorbents	Si/Al[a] at. ratio	Surface area (m^2/g)	External surface area (m^2/g)[e]	Pore volume (cm^3/g)[f]		
				Total	Micro	Meso
HY2.5	2.5	1063[b]	49[b]	0.39	0.36	0.03
HY2.9	2.9	897[b]	56[b]	0.39	0.30	0.09
USY22	22	932[b]	97[b]	0.51	0.31	0.20
USY33	33	928[b]	92[b]	0.47	0.28	0.19
USY40	40	937[b]	112[b]	0.52	0.31	0.21
ZSM-5	42	458	150	0.28	0.15	0.13
SiO_2	-	203[c]	203	1.13	-	1.13
ASA	54	352[c]	352	1.46	-	1.46
MCM-41	-	984[d]	984	0.65[d]	-	0.65[d]

Al_2O_3	-	326[c]	326	0.78	-	0.78
AC	-	1076[c]	34[c]	0.61	0.54	0.07

[a] Measured by ICP ; [b] Determined using Langmuir isotherm ; [c] Determined using BET nitrogen sorption ; [d] Determined using α-plot [36] ; [e] External surface = Surface of the outside of the zeolite grains and of the pores larger than 1.3 nm ; [f] Determined using t-plot

3.1.2 Hydroxyl groups

Figure 1 displays the IR spectra in the ν(OH) region of the most representative samples. HY2.5 features the well-known bands of bridged hydroxyls HF (high frequency) at 3645 cm^{-1} (supercages OH groups) and LF (low frequency) at 3550 cm^{-1} (sodalite cages OH groups) of the Y zeolite, whereas dealuminated HY2.9 zeolite shows the presence of three major additional OH bands at 3665, 3599 and 3535 cm^{-1} characteristic of the presence of the amorphous phase. The band at 3599 cm^{-1} is attributed in the literature to superacid hydroxyl groups obtained from the interaction between the OH groups of the supercage and the extraframework aluminum phase (EFAL) [37]. By analogy, the band at 3535 cm^{-1} can be attributed to sodalite cages OH groups perturbed by the EFAL phase, and the band at 3665 cm^{-1} is attributed to the OH groups of the EFAL phase. The steamed USY faujasites (only the spectra of USY22 is shown) displayed an intense sharp band at almost 3740 cm^{-1}, assigned to external silanol groups, in addition to low intense HF and LF ν(OH) bands, which is in a good agreement with their high Si/Al ratios. On ASA, SiO_2 and MCM-41, an intense and sharp SiOH band appears at 3747 cm^{-1}, with a broad signal that extends down to 3400 cm^{-1}, associated to H-bonded SiOH groups. The spectra of the ZSM-5 zeolite presents two bands: the first band at 3613 cm^{-1} is characteristic vibration of the framework OH groups whereas the second band at 3745 cm^{-1} is attributed to the terminal silanol groups of the external surface (Table 1) [40]. All these observations agree with the OH spectra expected for the various adsorbents.

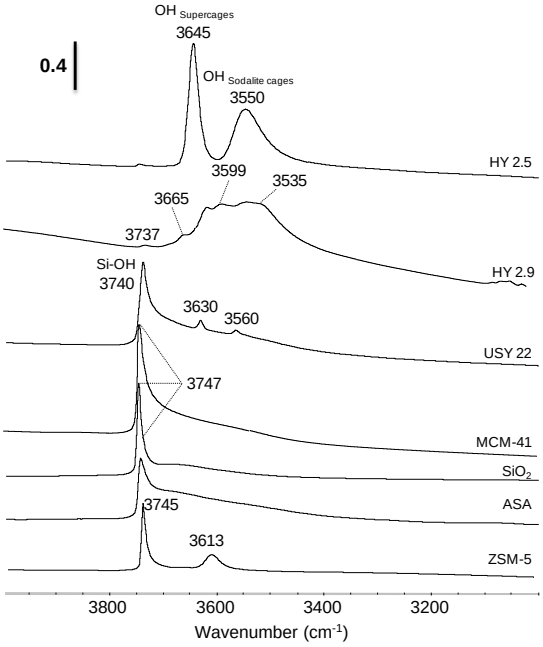

Figure 1 - Region of ν(OH) bands (3000 - 4000 cm^{-1}) of the different adsorbents after activation at 623 K under secondary vacuum.

The results of the quantification of the silanol groups, the HF and LF zeolitic OH groups of the various adsorbents are presented in Table 2. For silica-based samples, the amount of silanol groups increases with the surface area of these solids (Table 1). Over H-faujasites, the amount of silanol groups increases with the dealumination amount of the zeolitic framework (from 0 mmol of silanol per gram of HY2.5 zeolite up to 1.5 mmol of silanol per gram of USY40 zeolite). The formation of these silanol groups is related to the extraction of an aluminum atom from the zeolite structure that creates structural defects.

Table 2 - Amount of silanol groups, zeolitic OH groups and acid sites over the various solids, as determined by IR spectroscopy.

Adsorbent	Amount of OH groups (µmol/g)*			Amount of acid sites (µmol/g)*		
	SiOH	Supercage	Sodalite cage	BAS	LAS	Total
HY2.5	E	1160	2040	1263	22	1285
HY2.9	E	nd	nd	772	109	881
USY22	1210	45	58	136	189	325
USY33	1500	30	22	101	62	163
USY40	1550	22	25	60	17	77

ZSM-5	Nd	255#	-	240	42	282
SiO_2	1360	-	-	0	0	0
ASA	2320	-	-	14	71	85
MCM-41	3460	-	-	0	0	0

ε: Negligible; nd = not determined; # Framework OH groups; *: Data error analysis ± 6 %.

3.1.3 Acid sites

The pyridine adsorption spectra, of the most representative samples, are shown in the Figure SI-1. HY2.5 presents almost exclusively BAS sites (bands at 1630-1620 and at 1545 cm^{-1}). The amount of BAS detected on this sample is consistent with the amount of supercage OH groups detected (Table 2 – 1263 µmol/g BAS in comparison to 1160 µmol/g supercage OH groups). This points out that pyridinium ions cannot be formed over the sodalite OH groups of HY zeolite in particular for steric reasons [41]. Very few Lewis acid sites are detected on this sample in agreement with its absence of extraframework phase.

Over HY2.9 zeolite, pyridine adsorption confirms its dealumination by the detection of large amount of LAS (109 µmol/g - Table 2). Pyridinium species are also present, however, the comparison with the amount of the OH groups in supercages and sodalite cages is not possible regarding the complexity of the IR spectrum (Figure 1).

For USY zeolites, the amount of pyridinium species formed is strongly smaller than for the parent HY2.5. This is consistent with the decrease of the amount of the zeolitic OH groups, due to dealumination. It should be noted that comparison between pyridinium species amount and concentration of OH groups reveals that the amount of BAS is greater to the total amount of supercage plus sodalite OH groups (USY22 - OH groups of supercage + sodalite cages = 103 µmol/g; BAS = 136 µmol/g). Hence, contrary to HY, the strong acidic character of the zeolitic OH group of the dealuminated samples increases the mobility of the proton. This enables the protonation of pyridine molecules by the OH groups located in the sodalite cages [37]. The presence of acidic OH groups on the extraframework ASA phase of the USY zeolites should explained the greater amount of BAS detected compared to the amount of zeolitic OH groups [42]. The presence of some extraframework

phase is confirmed by the detection of strong LAS over USY. We can note that, as expected, the strength of Brønsted acid sites increases with the dealumination of zeolite [43,44].

The ZSM-5 zeolite presents both Brønsted and Lewis acid sites, as evidenced by the bands respectively at 1547 and 1456 cm^{-1}, giving a total number of 282 µmol/g of acid sites. The amount of Brønsted acid sites and that of zeolitic OH groups are in good agreement (240 µmol/g OH per versus 282 µmol/g acid sites). Over the SiO_2 and the MCM-41, no acid sites were detected which is in a good agreement with the non-presence of aluminum atoms in these samples. In the case of ASA solid, low amount of BAS and LAS was detected, as consequence with the high Si/Al ratio of this sample (Si/Al = 54).

3.2 Phenol adsorption capacities

3.2.1 Pretreatment effect on the phenol adsorption

As shown in Table 2, all the studied zeolites present acid sites, that are known by their affinity toward water adsorption [15,17]. Hence, the inhibitory effect of water on adsorbents over the phenol adsorption was studied on zeolites and mesoporous MCM-41 silica in batch reactor.

In batch reactor, thermal treatments were performed in two different conditions. Firstly, *ex-situ* pretreatment was performed to remove water from the adsorbents (623 K - 4h under Argon flow). The pretreated solid was then quickly transferred under air atmosphere to the hydrocarbon solution. In a second experiment, adsorbents were treated similarly using a home-built pretreatment cell (Figure SI-2) that allows the transfer of the adsorbents, into the hydrocarbon solution, under inert atmosphere (Argon), to avoid any water re-adsorption (*in-situ* pretreatment). Table 3 compares the amount of adsorbed phenol measured for different adsorbents, after following different pre-treatments conditions. Whatever *ex-situ* or *in-situ*, the pretreatment improves the adsorption capacity of all the studied adsorbents except for MCM-41 (Table 3). The type of the pretreatment setup (*ex-situ* or *in-situ*) did not lead to any beneficial effect over MCM-41 as well as over the zeolites with low aluminum loading. Conversely, the *in-situ* pretreatment appears to be recommended to reach the maximum adsorption capacity over high Al loaded zeolites. In the case of the *ex-situ* pretreatment, the short contact time of

these latter zeolites with the air moisture is enough to decrease their capacity toward phenol adsorption (Table 3). Figure 2 points out a direct correlation between the negative effect of the water contact on the amount of adsorbed phenol and the total amount of acidic sites (LAS + BAS - Table 2). Indeed, the phenol interaction energy with the protonic sites of H-faujasite (-85 kJ/mol), calculated using Grand Canonical Monte Carlo (GCMC) simulations, was found to be close to water interaction energy over the same site (-87.6 kJ/mol) [15]. Similar findings were observed by DFT calculations for the phenol and water interaction energies over extraframework LAS model (-199 kJ/mol for phenol in comparison to -190 kJ/mol for water) [34]. Thus, phenol molecules cannot displace all the water molecules, if these latter were already adsorbed on the acidic sites. We should mention that the absence of pretreatment effect for the MCM-41 agrees with the absence of any strong or medium acidic sites, as detected by pyridine adsorption (Table 2).

Table 3 - Effect of the pretreatment conditions on the phenol adsorption capacity for the different adsorbents in batch reactor.

	Amount of adsorbed phenol in batch reactor (mmol/g)		
Adsorbents	No pretreatment	*Ex-situ* retreatment	*In-situ* pretreatment
HY2.5	0.64	1.15	2.18
USY22	1.35	1.42	1.79
USY33	1.71	1.90	1.97
USY40	1.85	1.97	2.07
MCM-41	3.77	3.74	3.72

Experiments performed under batch conditions points out that the pretreatment conditions (*in-situ*, *ex-situ*, no pretreatment) can strongly modify the adsorption capacity of the adsorbent. The more hydrophilic the zeolite is (low Si/Al ratio), the stronger is the inhibitory effect of water. This result is consistent with the numerous studies that points out the importance of hydrophobic character for phenol removal from wastewater [17,45]. Thus, as shown for HY2.5, even a very short contact with air atmosphere largely rehydrates the adsorbent and spoils its adsorption capacity (Table 3). Since the *in-situ* pretreatment can strongly improve the adsorption capacities (more than a factor 3 for HY2.5), in all the following experiments, solids were *in-situ* pre-treated prior adsorption tests.

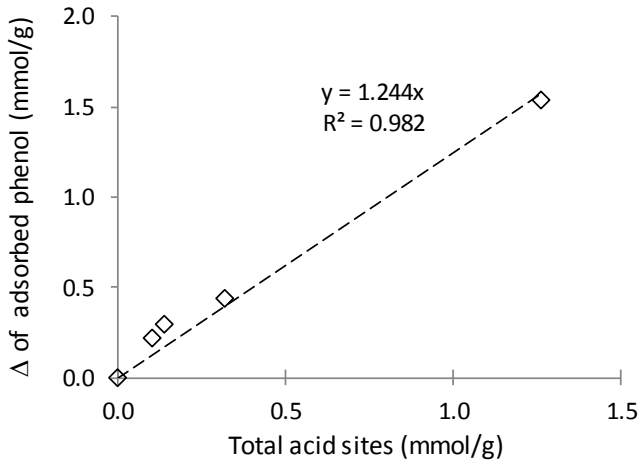

Figure 2 - Relation between the total amount of acid sites and the influence of the pretreatment over the different adsorbents. Δ = amount of adsorbed phenol with *in-situ* pretreatment at 623K minus amount of adsorbed phenol without pretreatment (batch reactor).

3.2.2 Phenol adsorption in the batch reactor

Figure 3 presents the adsorbed amounts of phenol by the different adsorbents, in batch reactor after *in-situ* activation at 623 K. Whatever the adsorbent, the adsorption phenomena is fast, and the equilibrium state is reached within few minutes. Figure 3 gives the percentage of phenol adsorbed after 1 hour over the various solids. In term of adsorption capacity, the most efficient adsorbents were mesoporous silica (MCM-41) and activated carbon, with almost 3.75 mmol of adsorbed phenol per gram of solid. For the silica-based solids (SiO_2, ASA, MCM-41), the amount of adsorbed phenol is related to their surface area of these materials, as shown in Figure 4. The maximum adsorption capacity was obtained for MCM-41 that possesses the highest surface area in this series (984 m^2/g). However, Y zeolites that also present high surface areas (937 - 1015 m^2/g), have shown lower performances. Whatever their Si/Al ratio, all the H-faujasites present similar adsorption capacities (between 1.79 and 2.18 mmol/g), except for the HY2.9 zeolite that shows greater adsorption capacity (3.07 mmol/g). The high adsorption capacity of HY2.9 zeolite, in comparison to HY2.5 zeolite, can be caused by its relative higher accessibility obtained from the creation of mesoporous cavities (Table 1). The amount of adsorbed phenol over ZSM-5 zeolite (1.88 mmol/g) was similar to that obtained over the HY2.5 and USY zeolites. By contrast, ZSM-5 is the only adsorbent over which the n-nonane molecules were also adsorbed. This can be due to the small apertures of ZSM-5 pores (5.5 x 5.1 Å)

that limit the accessibility of phenol molecules (kinetic diameter = 5.6 Å), in comparison to the big apertures of the Y zeolites supercages (7.4 x 7.4 Å) [46]. These small pores, non-filled with phenol, will be only accessible to the linear molecules, such as n-nonane. Hence, contrary to the Y zeolites, the ZSM-5 structure is not selective toward phenol adsorption in presence of linear hydrocarbons. Consequently, the ZSM-5 zeolite will not be studied in the flow adsorption section.

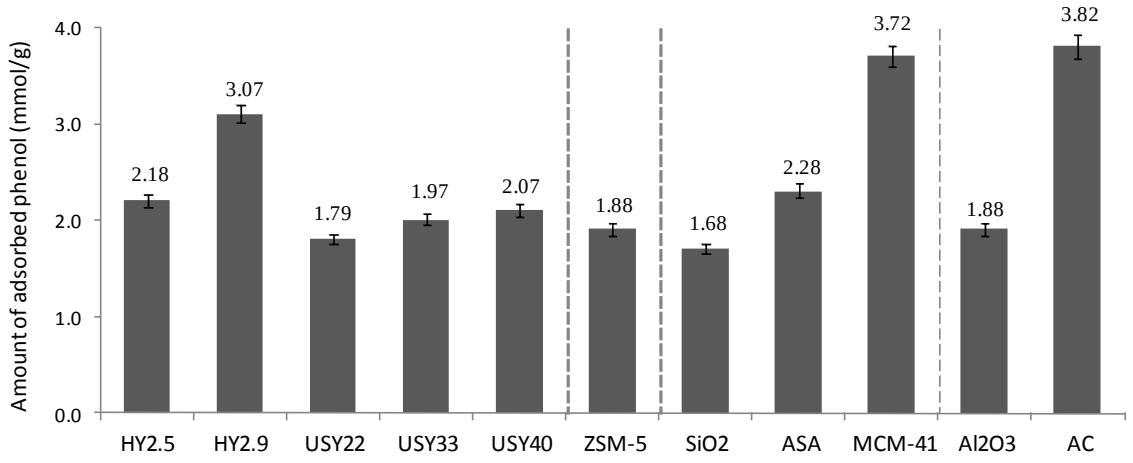

Figure 3 - Amount of adsorbed phenol from isooctane and 1 wt.% n-nonane mixture (C_{phenol} = 74.4 mmol/L ; V = 20 mL) over the different solids after 1 h in batch reactor. The error bar values (3%) were calculated by carrying out 3 experiments under the same conditions.

Two main parameters should affect the phenol adsorption capacities of the adsorbents: *(i)* textural properties (the surface area, the porous volume and the pores size) and *(ii)* acidic properties (nature, strength, amount and accessibility of the acid sites).

Effect of the textural properties

As previously reported on a series of faujasite [33], the amount of phenol adsorbed on HY and USY strongly depends on the microporous volume of their supercages. Whatever the H-faujasite considered, a constant value of 3 phenol molecules per supercage was depicted through both experimental studies and theoretical calculations. On activated carbon that mainly presents micropores, the adsorption of phenol is due to capillary condensation inside the micropores. Nevertheless, phenol can be also adsorbed into the mesopores, as shown by the high adsorption capacities obtained on the solids that do not present any micropore system i.e. SiO_2, ASA and MCM-41 (Table 1 and Figure 3). Over these adsorbents, no correlation could be obtained between the

amounts of phenol and the mesoporous volume (not shown) whereas a good link with the surface area of the adsorbents was observed (Figure 4; circle). Hence the greater the specific surface of mesoporous solids, the greater the amount of phenol adsorbed.

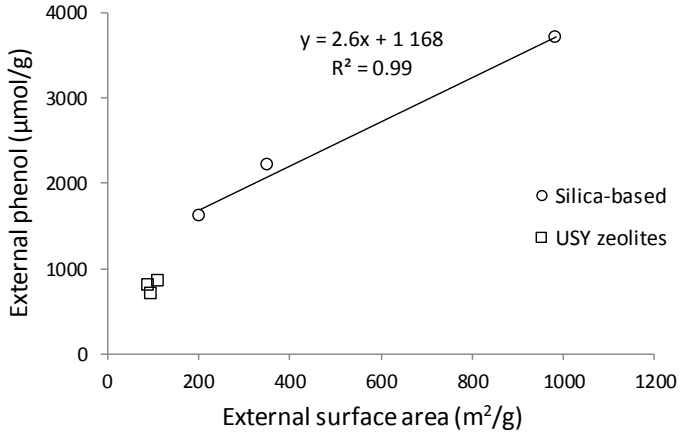

Figure 4 - Relationship between the amount of external phenol adsorbed (= total adsorbed phenol minus phenol adsorbed in micropores) and the external surface area of silica-based adsorbents and USY zeolites. Mixture of isooctane and 1wt.% n-nonane in batch reactor.

For USY zeolites that present both microporous and mesoporous systems, the amount of phenol specifically adsorbed into the micropores or into the mesopores can be assessed. Considering the total amount of adsorbed phenol and the fraction of microporous volume into the total porous volume ($V_{micropores}/V_{total}$), the quantity of "internal" phenol was calculated as reported in a previous work [33]. Consequently, from the total amount of adsorbed phenol and from the amount of "internal" phenol, the amount of "external" phenol can be deduced (External phenol = Total phenol - internal phenol) (Table 4). For all the USY samples, the amount of "external" phenol represents more than 60% of the total amount of phenol adsorbed. Table 4 pointed out that the ratios between the amount of "external" phenol and external surface stays close (~5 phenol molecules per nm^2).

Table 4 - Density of "external" phenol on the external surface of USY zeolites.

Zeolites	Total phenol (µmol/g)	Internal phenol (µmol/g)	External phenol (µmol/g)	External surface (m^2/g)	External phenol (molecules/nm^2)
USY22	1790	1088	702	97	4.4
USY33	1970	1174	796	92	5.2
USY40	2070	1234	836	112	4.5

Effect of the surface sites

The nature and the amount of superficial sites can also influence the adsorption phenomena. Indeed, a comparison of the amount of adsorbed phenol and the amount of silanol groups of silica-based samples shows a linear regression, that goes through the origin point (Figure 5). Moreover, from the value of the slope of the correlation (≈ 1), we can correspond one adsorbed phenol molecule to one silanol group. Table 1 and Table 2 allow us to calculate the density of silanol per square nanometer. It appears that the silanol density is lower on MCM-41 (2 SiOH/nm^2) than on silica and ASA (4 SiOH/nm^2) [47,48]. The variation of silanol group density among the silica-based sample explains why the relationship presented Figure 4 does not go through the origin point. Hence, these observations identify the increase in the density of silanol groups of silica-based samples as a key parameter to improve their phenol adsorption capacity.

As for silanol groups of the USY zeolites, it has been previously reported that on dealuminated zeolites, ν(SiOH) band at 3740 cm^{-1} characterizes both external silanol (located in the mesopores and on the outside surface of the zeolite grains) and internal silanol groups (defect sites of the supercage and sodalite cages). These latter although not accessible, appears at the same frequencies than external SiOH. Hence the amount of the silanol groups of USY reported on Figure 5 comprised both internal and external SiOH groups. This explains why the total amount of silanol groups does not correlated with the amount of external phenol. Thus, from this graph (see arrows of Figure 5), one can estimated that the amount of silanol exceeding the linear correlation (= total silanol - external phenol) can be attributed to internal silanol groups. This can be proposed as a method for determining the accessibility of silanol groups of such zeolites.

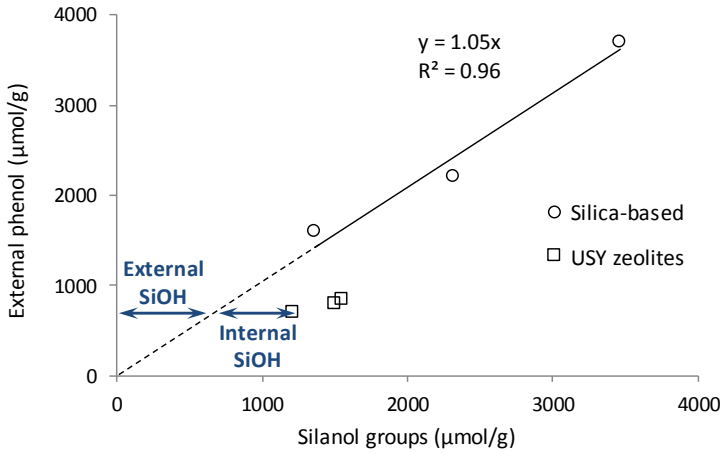

Figure 5 - Relationship between the amount of external phenol (= total adsorbed phenol minus internal phenol) and the amount of silanol groups of silica-based adsorbents and USY zeolites.

3.2.3 Phenol adsorption in flow reactor

The adsorption in a flow reactor is the most commonly adsorption method used in the industries. This method has the double advantages of making easier the *in-situ* activation of the adsorbent as well as its re-use for several adsorption runs after its *in-situ* regeneration between each two cycles. Only a selection of specific adsorbents was tested under flow conditions. In addition to MCM-41 (only silanol groups), alumina (strong acid sites) and activated carbon (reference adsorbent), a selection of Y zeolites was studied under these conditions. The zeolites were chosen in order to compare the effects of the Si/Al ratio and the acidity (and ratio) of the different OH groups (zeolitic OH groups and silanol groups).

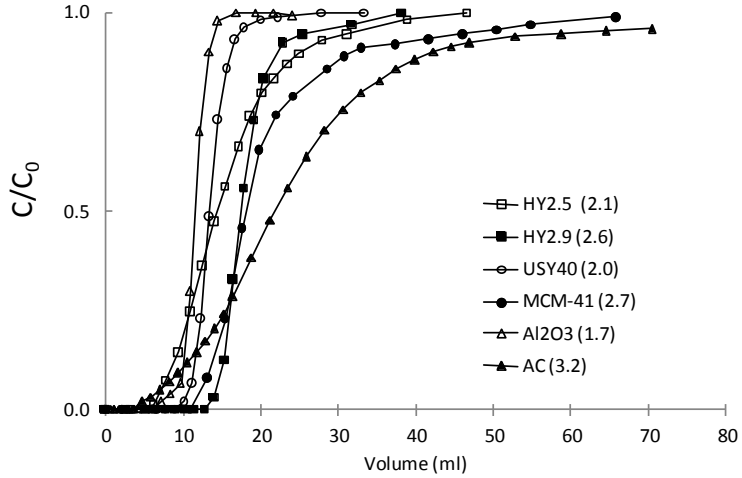

Figure 6 - Breakthrough curves of the phenol adsorption from isooctane mixture over the different adsorbents (C_0 = 74.4 mmol/L). Between the brackets is given the amount of adsorbed phenol over each adsorbent in mmol/g.

Figure 6 compared the breakthrough curves of the adsorbents for a phenol concentration of 74.4 mmol/L in isooctane and 1 wt.% n-nonane. Using the formula (F1), from the section 2.3, and the specific retention time for each adsorbent, the amount of adsorbed phenol at saturation was calculated for each solid (Figure 7 - Cycle 1). Similar trends were observed in flow and batch conditions. The Si/Al ratio does not affect the adsorption capacity of HY2.5, and USY40 (~2 mmol/g) and HY2.9 still presents the greatest adsorption capacities (2.6 mmol/g) among the zeolite samples. A comparison of the mass-transfer zone or, equivalently, the difference between breakthrough and equilibration times, for HY2.5 and HY2.9 zeolites shows a shorter mass-transfer zone over the HY2.9 zeolite. The shorter the mass-transfer is, the most efficient is the adsorbent. The short mass-transfer zone of the HY2.9 zeolite can be the reason of the higher accessibility, and thus the higher adsorption capacity, of HY2.9 zeolite in comparison to HY2.5 zeolite. Al_2O_3 presents a lower adsorption capacity (1.7 mmol/g) compared to the other adsorbents, while MCM-41 and activated carbon maintained their high adsorption capacities with 2.7 and 3.2 mmol of adsorbed phenol per gram of solid, respectively. Hence, if the amount of adsorbed phenol was the only considered parameter, activated carbon would be considered as the best adsorbent. This result is not surprising since activated carbon is known for its high capacity of adsorption due to its high surface area and the capillary condensation occurring inside the pores [17,27,49]. However, another important parameter must be considered for larger scale

adsorption application: "*the breakthrough time* (t_B)", that corresponds to the time during which the solids produce ultra-clean biofuel by adsorbing all the phenol molecules from the solution. Indeed, within the objective of developing an industrial process, the adsorption time during which ultra-pure biofuels are obtained (phenol molecules are completely removed) is the most important parameter. Figure 6 points out that the shape of the breakthrough curves can be very different as between the 3 most performant adsorbents: HY2.9, MCM-41 and activated carbon. The activated carbon presents the shortest breakthrough time - t_B = 4 min. However, the phenol diffusion into the pores of activated carbon is slow and adsorption requires almost 50 minutes before reaching saturation. Otherwise, the breakthrough time is greater over MCM-41 - t_B = 11 min and similarly, due the low diffusion rate, the saturation takes almost 60 min to get reached. By contrast, HY2.9 zeolite was able to produce ultra-clean biofuel during 13 min, exceeding the breakthrough time of MCM-41 and activated carbon. A comparison between the adsorption capacities of HY2.9, MCM-41 and activated carbon using specific retention times and breakthrough times is shown in Table 5. By looking to the amount of phenol adsorbed at the breakthrough time, the zeolite HY2.9 shows the most promising results (1.9 mmol/g) in terms of providing the largest amount of ultrapure biofuel in one adsorption cycle, followed by the MCM-41 (1.3 mmol/g) and the USY40 zeolite (1.6 mmol/g), whereas the adsorption capacity of activated carbon drops to not more than 0.6 mmol/g, as shown in Table 5.

Table 5 - Comparison between the amounts of phenol adsorbed using retention and breakthrough values for the most promising adsorbents.

Adsorbents	Retention values		Breakthrough values	
	t_R (min)	Adsorbed phenol (mmol/g)	t_B (min)	Adsorbed phenol (mmol/g)
HY2.9	17.7	2.6	13	1.9
USY40	13.4	2.0	9	1.3
MCM-41	18.3	2.7	11	1.6
AC	21.3	3.2	4	0.6

3.3 Regeneration capacity of the adsorbents

The regeneration ability of the solids was studied on two adsorption-desorption cycles. To remove phenol molecules adsorbed after cycle 1, a thermal desorption under Argon flow (90 cm^3/min) at 473 K for 4 hours was applied. After returning to 298 K, a second adsorption cycle was performed in the same conditions as the first. Adsorption capacities of cycles 1 and 2 were compared in Figure 7.

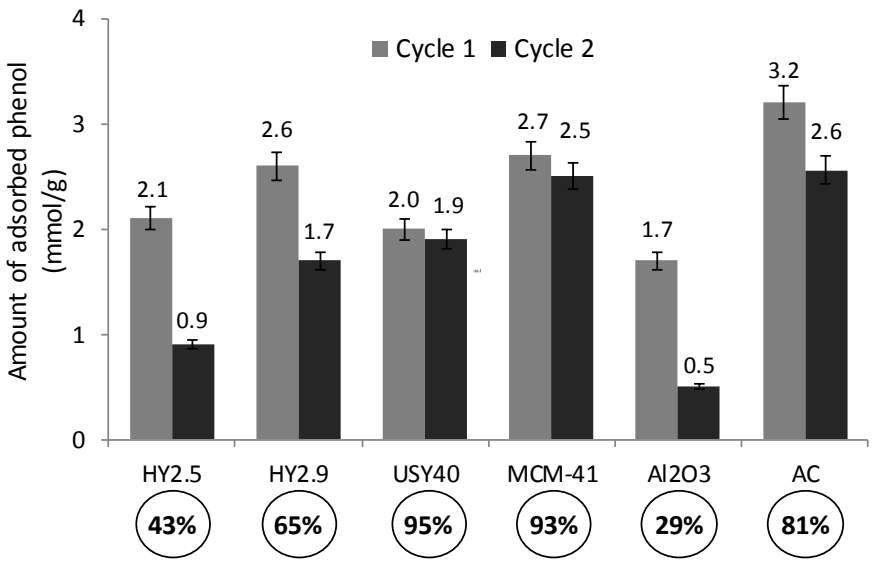

Figure 7 - Amount of adsorbed phenol over two consecutives adsorption cycles. Values in circles correspond to the regeneration percentages between the two adsorption cycles after a desorption step of 4 hours at 423K under Argon flow.

Figure 7 points out that Al_2O_3 presents the lowest regeneration capacity (29%). This is in line with previous studies that showed that chemisorption of phenol over the strong Lewis acid sites of alumina leads to the formation of phenolates species strongly held on surface [50]. By contrast, the activated carbon presents a somewhat high regeneration capacity (81%) that is line with the phenol condensation into AC micropores. After two adsorption cycles, AC presents equivalent adsorption capacity than MCM-41. MCM-41 presents very high regeneration capacity equal to 93% over 2 adsorption cycles which is explained by the interaction of phenol molecules with the very weakly acidic silanol groups located into the mesopores of MCM-41

Over the H-zeolites, the regeneration capacity increases with the Si/Al ratio (HY: 43%; HY2.9: 65%; USY40: 95%). As shown in Figure SI-4, the amount of residual phenol (non-desorbed phenol species by treatment at 473K) directly depends of the amount of acidic sites of the zeolites (BAS + LAS

quantified in Table 2) [33]. Hence, the presence of strongly acidic OH groups of the zeolites and Lewis acid sites (Al^{3+}) limit the regeneration capacity of the different zeolites.

The results on the various zeolites also reveal that, for given conditions of regeneration, regenerability changes with the amount of OH groups but not with their acidic strength. Once the strength is above a certain value (in the present case: greater than that of silanol), the regeneration is limited.

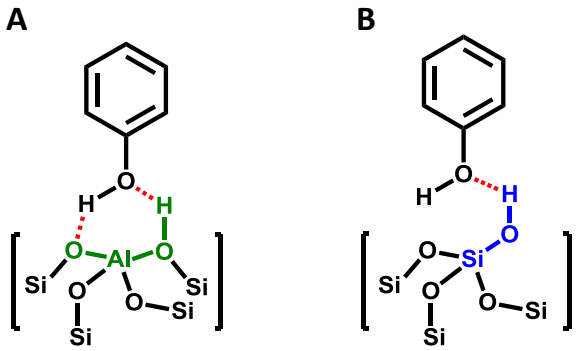

Figure 8 - Scheme for phenol adsorption on A) Acidic OH groups of zeolites; B) External silanol groups of silica-based samples and USY zeolites.

From the adsorption and regeneration properties, mechanisms for phenol adsorption on MCM and H-faujasite can be proposed in Figure 8. For silica-based samples, the relationship between the amount of phenol adsorbed and that of silanol groups (Fig. 5) indicates that one phenol is H-bonded to one silanol groups, as depicted in Figure 8-B. The interaction with weakly acidic silanol groups is also confirmed by the good regeneration capability of the MCM.

On the Y zeolites, the greater the amount of acidic sites, the lower the capability of regeneration (Figure SI-4). This indicates that phenol interacts with zeolitic OH groups. This agrees with the DFT computed model in a previous study [33], that shows that phenol interacts by its oxygen atom with the proton zeolitic of the zeolite as depicted in Figure 8-A. The zeolitic OH group acidic strength being greater than that of silanol groups, they retain more strongly the phenol, limiting the regeneration capacity of Y zeolites with low Si/Al ratio.

These sections allow identifying the most promising adsorbents considering their adsorption and regeneration capacities. The challenge that arises now concerns the selectivity of these adsorbents toward phenol into a more complex hydrocarbon mixture containing an aromatic compound.

3.4 Selective phenol adsorption in presence of toluene

The selectivity toward phenol adsorption was tested under flow conditions from a mixture of 1 wt.% phenol (74.4 mmol/L), 1 wt.% n-nonane and different concentrations of toluene (1 - 40 wt.%) into isooctane. In a first step, the experiments were performed by flowing a solution of isooctane + 1 wt.% n-nonane containing similar weight amount of phenol and toluene (1 wt.%) over a column filled with 0.5 g of the studied adsorbents. Six adsorbents were tested: HY2.5, HY2.9 and USY40 (to account for the effect of the Si/Al ratio and absence/presence of EFAL phase), MCM-41 (to account for the selectivity of the silanol groups), Al_2O_3 (to account for the selectivity of the aluminum coordinative unsaturated sites) and activated carbon as a reference. The obtained breakthrough curves for phenol and toluene are shown in Figure 9. Over all the series of adsorbents, initially phenol and toluene are both adsorbed. However, toluene is eluted very rapidly and before the breakthrough of phenol. Phenol adsorption is preferred over toluene for all adsorbents. It should be noted that at the beginning of the toluene elution, a roll-up effect appears i.e. the concentration of toluene in the liquid phase is greater than in the initial solution. This is explained by the fact that phenol molecules displace the already adsorbed toluene molecules, and thus, the toluene concentration in the effluent surpass temporarily that of the feed.

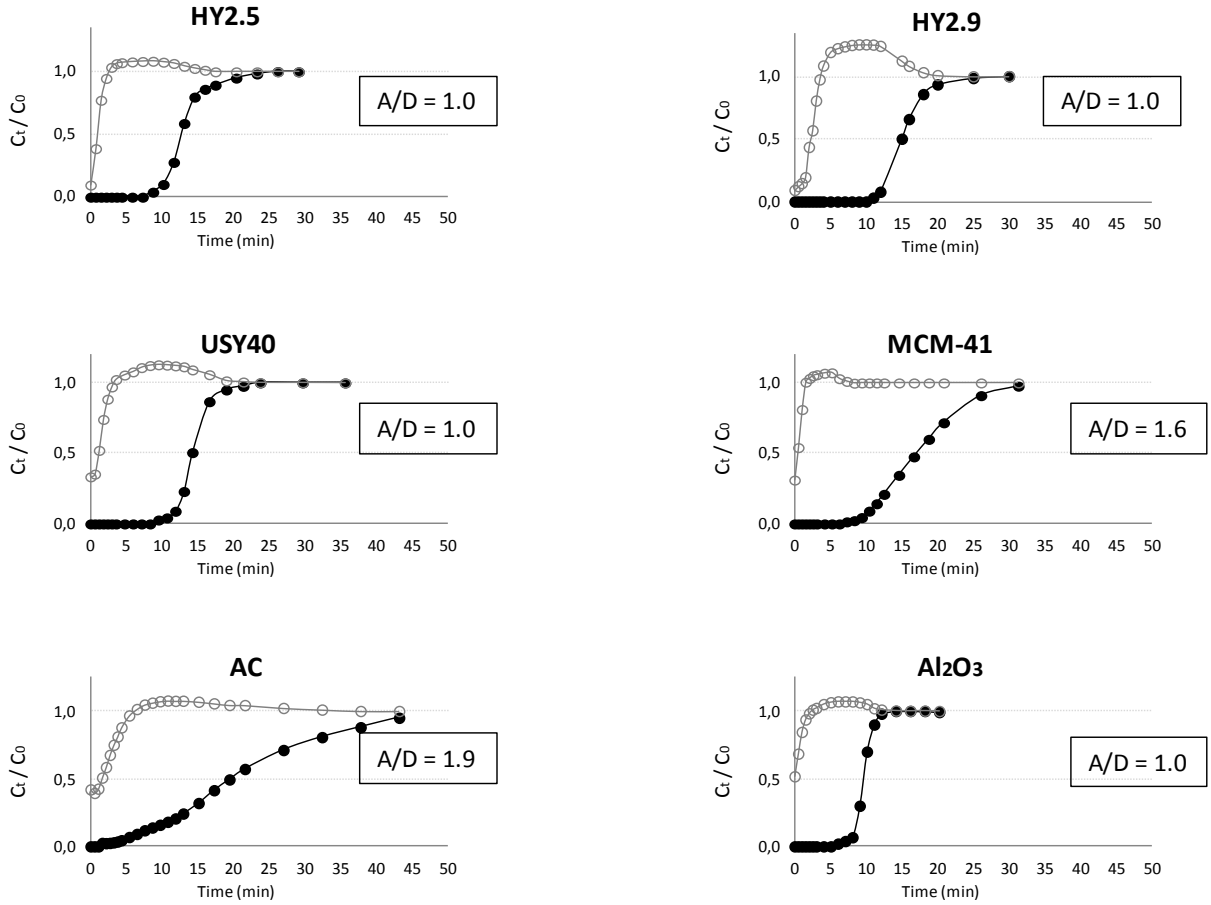

Figure 9 - Breakthrough curves of phenol/toluene co-adsorption over various adsorbents. Full circle = Phenol; Open circle = toluene. A/D represents the ratio of the areas of adsorbed (A) and displaced (D) toluene (see Supplementary Information Figure SI-5).

Even if all the solids show this roll-up effect for toluene indicating their preferential adsorption for phenol, its extent depends on the adsorbents. The ratio of the adsorbed toluene over the displaced toluene (A/D) was calculated for the various adsorbents by integrating the zones of adsorbed and displaced toluene as mentioned in Figure 9 (HY2.5).

Over activated carbon, the A/D value is 1.9 for a solution containing 1% toluene. This shows that activated carbon maintains some adsorbed toluene molecules in its cavities. Over activated carbon, the adsorption only occurs by capillary condensation inside the pores. Thus, there are no adsorption sites that can move the adsorption toward a specific molecule. For such a reason, the selectivity of activated carbon toward phenol is very weak in presence of toluene. As shown on Figure 9 and Table 6, the presence of toluene did not affect the adsorption capacity of Al_2O_3. Indeed, as mentioned before, phenol is so strongly adsorbed on alumina since the selectivity toward phenol reaches high values. On

protonated zeolite acid sites, HY2.5 (BAS), HY2.9 (BAS + LAS) as well as USY40 (lower amount of BAS and LAS), phenol completely displaced all the adsorbed toluene molecules (A/D ≈ 1). These results can be explained by the respective strength of adsorption of phenol and toluene molecules with the surface sites of the adsorbents. As shown previously by theoretical calculation on zeolites, the toluene molecules can only be adsorbed by their aromatic cycle whereas phenol molecules can be adsorbed both by their aromatic cycle or by their OH groups, even if this latter mode is favored [34]. Computed adsorption energy showed that, on zeolitic OH groups adsorption energy of phenol (-79 kJ/mol) is greater than that of toluene (-56 kJ/mol), confirming the preferential adsorption of phenol on protonic zeolites. Over weak acid Si-OH groups (MCM-41 and main superficial sites over USY40) the phenol is weakly adsorbed via its OH group; as confirmed by the high regeneration capacity of these solids (Figure 7). However, this weak interaction was strong enough to maintain a selective adsorption of phenol in presence of 1wt.% of toluene.

In a second step, the selectivity toward phenol adsorption was also tested with different mixtures containing higher amount of toluene (10 and 40 wt.%, this latter corresponds to the amount of aromatic compounds in second generation biofuels). The amount of adsorbed phenol was calculated, as in the previous section (using the formula F1) and results are given in Table 6. As for activated carbon, the increase of the concentration of toluene makes its poor selectivity more marked. Hence, activated carbon is not satisfying adsorbent to purify a mixture of hydrocarbons. As for Al_2O_3, whatever the toluene concentration, selectivity toward phenol remains intact. The less affected zeolites by the increase of the amount of toluene are HY2.5 and HY2.9 zeolites, which reports the high efficiency of strong acidic OH groups and LAS for the selective removal of phenol even in presence of large amount of aromatic compounds. Regeneration experiments under the aforementioned conditions (section 3.3) were also performed over HY2.5 and HY2.9 zeolites in presence of 40 wt.% toluene in the mixture (Figure SI-6). Similar regeneration capacities as in the case of absence of toluene were observed (45% and 63% for HY2.5 and HY2.9 zeolites, respectively).

Table 6 - Amount of adsorbed phenol, measured in the flow reactor, in presence of different concentrations of toluene.

	Amount of adsorbed phenol (mmol/g)			
Adsorbents	1% phenol 0% toluene	1% phenol 1% toluene	1% phenol 10% toluene	1% phenol 40% toluene
HY2.5	2.1	2.0	2.1	2.2
HY2.9	2.6	2.7	2.6	2.4
USY40	2.0	1.9	1.7	0.9
MCM-41	2.7	2.5	2.5	1.0
AC	3.2	2.7	1.7	0.4
Al_2O_3	1.7	1.7	1.6	1.6

Over MCM-41 and USY40, the selectivity of weak acidic Si-OH groups was maintained until a concentration of 10 wt.% of toluene in the solution. However, for 40 wt.% of toluene, the amount of adsorbed phenol markedly decreases over these 2 solids (from 2.0 to 0.9 mmol/g over USY40 and from 2.7 to 1.0 mmol/g over MCM-41). Since the adsorption being performed under dynamic conditions, toluene molecules present in large quantity in the flow may train the weakly adsorbed phenol molecules by π-π interaction (aromatic rings interaction). To verify this hypothesis, adsorption experiments were performed after substituting the toluene by methylcyclohexane (MCH) in order to remove the effect of the π-π interactions. Results, presented in Table 7, prove that the adsorption capacities for phenol of the MCM-41 and USY40 are not affected by the presence of methylcyclohexane. This confirms that a solvation effect occurs with π-π interaction of the molecules in the flow prevents the trapping of phenol on the weak adsorption sites (Si-OH groups) of the adsorbents.

Table 7 – Amount of adsorbed phenol over MCM-41 and USY40 in presence of 40 wt.% of toluene or MCH.

	Amount of adsorbed phenol (mmol/g)		
Adsorbents	1% phenol 0% toluene	1% phenol 40% toluene	1% phenol 40% MCH
USY40	2.0	0.9	1.9
MCM-41	2.7	1.0	2.8

CONCLUSION

The present study deals with the selective removal of phenol from a semi-model biofuel mixture. Various types of adsorbents i.e. Y, USY and ZSM-5 zeolites, silica-based oxides, aluminum oxide and activated carbon, that present different structural, textural and acidic properties were tested.

- Micropores and mesopores of the Y zeolites are both involved in the phenol adsorption although in a very different way. Phenol is condensed into the micropores of the Y zeolites and an amount of 3 phenol molecules per supercage was measured on the different faujasites. Such fraction of phenol called “internal phenol” is directly related to the porous volume of the crystalline fraction of the zeolite. In the same manner, AC with its great microporous network also presents high phenol adsorption capacities. Note that, in the zeolitic micropores with entrance lower than 6 Å, as for Y sodalite cage and ZSM-5 pores, the phenol adsorption is very limited. Additional amount of phenol, called “external phenol” are adsorbed on the silanol groups of the mesoporous cavities of the zeolites (created by dealumination). On silica-based solids that present only mesopores, the present study establishes that one phenol molecule interacts with one silanol group. Thus, the phenol adsorption capacity in the mesopores is directly correlated to the concentration of silanol groups.

- Acidic properties of the adsorbents strongly impact their selectivity. In presence of 1 - 10 wt.% toluene, HY and USY zeolites and MCM-41 present good phenol adsorption capacities. By contrast, a greater amount of toluene (40 wt.%) strongly decreases the selectivity for phenol adsorption over USY and MCM-41. This is explained by the solvation effect that affect the weak acidic silanol groups, largely present over these solids, and thus prohibits them from adsorbing phenol under such condition. Although activated carbon that presents high phenol adsorption capacities in simple mixture, has shown a very poor selectivity toward phenol in more complex hydrocarbon mixtures, due to the absence of acidic properties. Hence to selectively adsorbed phenol, large amount of strongly acidic sites is required as over HY2.5 and HY2.9 zeolites.

- Acidic properties were shown to negatively influence the regenerability of the adsorbents. To regenerate the adsorbents under mild conditions, the amount of strong Brønsted or Lewis acidic sites

must be limited since they strongly retain phenol. Thus, the best regeneration capacities are obtained on USY and MCM-41.

Hence, this study allows rationalizing the impact of the micro- and mesoporous texture as well as the location, nature and strength of the acidic sites on their adsorption capacities, selectivity and regeneration abilities. The best compromise between adsorption capacity, selectivity toward phenol and regeneration ability was obtained with HY2.9 zeolite, i.e. the solid that presents large amount of micropores, some mesopores and an intermediate amount of strongly acidic sites. This allows obtaining good adsorption capacity, maintaining a high selectivity and acceptable regeneration.

ACKNOWLEDGMENTS

We thank the Labex EMC3, ANR and FEDER for the PhD grant of IK and for the financial support to the BIOCAR project. We also thank Benjamin FOUCAULT and Adrien LANEL for helping in installation, design and realization of adsorption setup.

REFERENCES

[1] BP Energy Outlook 2018, (2018) 125.

[2] M. Bertero, G. de la Puente, U. Sedran, Fuels from bio-oils: Bio-oil production from different residual sources, characterization and thermal conditioning, Fuel. 95 (2012) 263–271. doi:10.1016/j.fuel.2011.08.041.

[3] M.N. Nabi, M.M. Rahman, M.A. Islam, F.M. Hossain, P. Brooks, W.N. Rowlands, J. Tulloch, Z.D. Ristovski, R.J. Brown, Fuel characterisation, engine performance, combustion and exhaust emissions with a new renewable Licella biofuel, Energy Conversion and Management. 96 (2015) 588–598. doi:10.1016/j.enconman.2015.02.085.

[4] G. Fogassy, N. Thegarid, Y. Schuurman, C. Mirodatos, From biomass to bio-gasoline by FCC co-processing: effect of feed composition and catalyst structure on product quality, Energy & Environmental Science. 4 (2011) 5068. doi:10.1039/c1ee02012a.

[5] S.S. Reham, H.H. Masjuki, M.A. Kalam, I. Shancita, I.M. Rizwanul Fattah, A.M. Ruhul, Study on stability, fuel properties, engine combustion, performance and emission characteristics of biofuel emulsion, Renewable and Sustainable Energy Reviews. 52 (2015) 1566–1579. doi:10.1016/j.rser.2015.08.013.

[6] J.C. Serrano-Ruiz, J.A. Dumesic, Catalytic routes for the conversion of biomass into liquid hydrocarbon transportation fuels, Energy and Environmental Science. 4 (2011) 83–99. doi:10.1039/C0EE00436G.

[7] G. Fogassy, C. Lorentz, G. Toussaint, N. Thegarid, Y. Schuurman, C. Mirodatos, Analytical techniques tailored for biomass transformation to biofuels, Environmental Progress & Sustainable Energy. 32 (2013) 377–383. doi:10.1002/ep.10631.

[8] F. de Miguel Mercader, M.J. Groeneveld, S.R.A. Kersten, N.W.J. Way, C.J. Schaverien, J.A. Hogendoorn, Production of advanced biofuels: Co-processing of upgraded pyrolysis oil in standard refinery units, Applied Catalysis B: Environmental. 96 (2010) 57–66. doi:10.1016/j.apcatb.2010.01.033.

[9] E.-M. Aro, From first generation biofuels to advanced solar biofuels, Ambio. 45 (2016) 24–31. doi:10.1007/s13280-015-0730-0.

[10] R. Chaudhary, P.L. Dhepe, Solid base catalyzed depolymerization of lignin into low molecular weight products, Green Chemistry. 19 (2017) 778–788. doi:10.1039/C6GC02701F.

[11] C. Bouvier, Y. Romero, F. Richard, S. Brunet, Effect of H2S and CO on the transformation of 2-ethylphenol as a model compound of bio-crude over sulfided Mo-based catalysts: propositions of promoted active sites for deoxygenation pathways based on an experimental study, Green Chemistry. 13 (2011) 2441. doi:10.1039/c1gc15181a.

[12] G.W. Huber, S. Iborra, A. Corma, Synthesis of Transportation Fuels from Biomass: Chemistry, Catalysts, and Engineering, Chemical Reviews. 106 (2006) 4044–4098. doi:10.1021/cr068360d.

[13] Z. Zhang, Q. Wang, P. Tripathi, C.U. Pittman Jr, Catalytic upgrading of bio-oil using 1-octene and 1-butanol over sulfonic acid resin catalysts, Green Chemistry. 13 (2011) 940. doi:10.1039/c0gc00464b.

[14] M. Bertero, U. Sedran, Upgrading of bio-oils over equilibrium FCC catalysts. Contribution from alcohols, phenols and aromatic ethers, Catalysis Today. 212 (2013) 10–15. doi:10.1016/j.cattod.2013.03.016.

[15] F. Ektefa, S. Javadian, M. Rahmati, Computational comparison of the efficiency of nanoporous zeolite frameworks for separation of phenol from water, Journal of the Taiwan Institute of Chemical Engineers. 88 (2018) 104–113. doi:10.1016/j.jtice.2018.03.020.

[16] B. Koubaissy, G. Joly, I. Batonneau-Gener, P. Magnoux, Adsorptive Removal of Aromatic Compounds Present in Wastewater by Using Dealuminated Faujasite Zeolite, Industrial & Engineering Chemistry Research. 50 (2011) 5705–5713. doi:10.1021/ie100420q.

[17] M. Khalid, G. Joly, A. Renaud, P. Magnoux, Removal of Phenol from Water by Adsorption Using Zeolites, Industrial & Engineering Chemistry Research. 43 (2004) 5275–5280. doi:10.1021/ie0400447.

[18] B. Van de Voorde, D. Damasceno Borges, F. Vermoortele, R. Wouters, B. Bozbiyik, J. Denayer, F. Taulelle, C. Martineau, C. Serre, G. Maurin, D. De Vos, Isolation of Renewable Phenolics by Adsorption on Ultrastable Hydrophobic MIL-140 Metal–Organic Frameworks, ChemSusChem. 8 (2015) 3159–3166. doi:10.1002/cssc.201500281.

[19] L. Damjanović, V. Rakić, V. Rac, D. Stošić, A. Auroux, The investigation of phenol removal from aqueous solutions by zeolites as solid adsorbents, Journal of Hazardous Materials. 184 (2010) 477–484. doi:10.1016/j.jhazmat.2010.08.059.

[20] W. Kujawski, A. Warszawski, W. Ratajczak, T. Porebski, W. Capa\la, I. Ostrowska, Removal of phenol from wastewater by different separation techniques, Desalination. 163 (2004) 287–296.

[21] S. Petkovic, B. Adnadjevic, J. Jovanovic, Novel kinetics model for adsorption of pollutant from wastewaters onto zeolites. Kinetics of phenol adsorption on zeolite-type silicalite, Adsorption Science & Technology. 37 (2019) 349–364. doi:10.1177/0263617419833201.

[22] O. Hamdaoui, E. Naffrechoux, Modeling of adsorption isotherms of phenol and chlorophenols onto granular activated carbonPart II. Models with more than two parameters, Journal of Hazardous Materials. 147 (2007) 401–411. doi:10.1016/j.jhazmat.2007.01.023.

[23] G.D. Sheng, D.D. Shao, X.M. Ren, X.Q. Wang, J.X. Li, Y.X. Chen, X.K. Wang, Kinetics and thermodynamics of adsorption of ionizable aromatic compounds from aqueous solutions by as-prepared and oxidized multiwalled carbon nanotubes, Journal of Hazardous Materials. 178 (2010) 505–516. doi:10.1016/j.jhazmat.2010.01.110.

[24] N.A. Khan, Z. Hasan, S.H. Jhung, Adsorptive removal of hazardous materials using metal-organic frameworks (MOFs): A review, Journal of Hazardous Materials. 244–245 (2013) 444–456. doi:10.1016/j.jhazmat.2012.11.011.

[25] B.H. Hameed, A.A. Rahman, Removal of phenol from aqueous solutions by adsorption onto activated carbon prepared from biomass material, Journal of Hazardous Materials. 160 (2008) 576–581. doi:10.1016/j.jhazmat.2008.03.028.

[26] T. Viraraghavan, F. de Maria Alfaro, Adsorption of phenol from wastewater by peat, fly ash and bentonite, Journal of Hazardous Materials. 57 (1998) 59–70. doi:10.1016/S0304-3894(97)00062-9.

[27] N. Roostaei, F.H. Tezel, Removal of phenol from aqueous solutions by adsorption, Journal of Environmental Management. 70 (2004) 157–164. doi:10.1016/j.jenvman.2003.11.004.

[28] D. Hank, Z. Azi, S. Ait Hocine, O. Chaalal, A. Hellal, Optimization of phenol adsorption onto bentonite by factorial design methodology, Journal of Industrial and Engineering Chemistry. 20 (2014) 2256–2263. doi:10.1016/j.jiec.2013.09.058.

[29] S. Babel, Low-cost adsorbents for heavy metals uptake from contaminated water: a review, Journal of Hazardous Materials. 97 (2003) 219–243. doi:10.1016/S0304-3894(02)00263-7.

[30] T. Mathialagan, T. Viraraghavan, Adsorption of cadmium from aqueous solutions by perlite, Journal of Hazardous Materials. 94 (2002) 291–303. doi:10.1016/S0304-3894(02)00084-5.
[31] F.P. Lobban, Process for removing phenols and mercaptans from light petroleum distillates, US patent 2605212, 1952.
[32] R.C. Schlicht, F.C. Mccoy, Selective adsorption of phenols from solution in hydrocarbons, US Patent 3617531, 1971.
[33] I. Khalil, H. Jabraoui, G. Maurin, S. Lebègue, M. Badawi, K. Thomas, F. Maugé, Selective Capture of Phenol from Biofuel Using Protonated Faujasite Zeolites with Different Si/Al Ratios, The Journal of Physical Chemistry C. 122 (2018) 26419–26429. doi:10.1021/acs.jpcc.8b07875.
[34] H. Jabraoui, I. Khalil, S. Lébegue, M. Badawi, Ab Initio Screening of Cation-Exchanged Zeolites for Biofuel Purification, Molecular Systems Design & Engineering. (2019) 10.1039.C9ME00015A. doi:10.1039/C9ME00015A.
[35] M. Grün, K.K. Unger, A. Matsumoto, K. Tsutsumi, Novel pathways for the preparation of mesoporous MCM-41 materials: control of porosity and morphology, Microporous and Mesoporous Materials. 27 (1999) 207–216. doi:10.1016/S1387-1811(98)00255-8.
[36] M. Kruk, M. Jaroniec, C.H. Ko, R. Ryoo, Characterization of the Porous Structure of SBA-15, Chemistry of Materials. 12 (2000) 1961–1968. doi:10.1021/cm000164e.
[37] S. Khabtou, T. Chevreau, J.C. Lavalley, Quantitative infrared study of the distinct acidic hydroxyl groups contained in modified Y zeolites, Microporous Materials. 3 (1994) 133–148. doi:10.1016/0927-6513(94)00015-8.
[38] H. Li, S.A. Kadam, A. Vimont, R.F. Wormsbecher, A. Travert, Monomolecular Cracking Rates of Light Alkanes over Zeolites Determined by IR Operando Spectroscopy, ACS Catalysis. 6 (2016) 4536–4548. doi:10.1021/acscatal.6b01025.
[39] J.-P. Gallas, J.-M. Goupil, A. Vimont, J.-C. Lavalley, B. Gil, J.-P. Gilson, O. Miserque, Quantification of Water and Silanol Species on Various Silicas by Coupling IR Spectroscopy and in-Situ Thermogravimetry, Langmuir Article. 25 (2009) 5825–5834.
[40] P.A. Jacobs, R. Von Ballmoos, Framework hydroxyl groups of H-ZSM-5 zeolites, The Journal of Physical Chemistry. 86 (1982) 3050–3052. doi:10.1021/j100212a046.
[41] F. Thibault-Starzyk, B. Gil, S. Aiello, T. Chevreau, J.-P. Gilson, In situ thermogravimetry in an infrared spectrometer: an answer to quantitative spectroscopy of adsorbed species on heterogeneous catalysts, Microporous and Mesoporous Materials. 67 (2004) 107–112. doi:10.1016/j.micromeso.2003.10.016.
[42] O. Cairon, T. Chevreau, J.-C. Lavalley, Brønsted acidity of extraframework debris in steamed Y zeolites from the FTIR study of CO adsorption, Journal of the Chemical Society, Faraday Transactions. 94 (1998) 3039–3047.
[43] K. Thomas, C. Binet, T. Chevreau, D. Cornet, J.-P. Gilson, Hydrogenation of Toluene over Supported Pt and Pd Catalysts: Influence of Structural Factors on the Sulfur Tolerance, Journal of Catalysis. 212 (2002) 63–75. doi:10.1006/jcat.2002.3780.
[44] G. Crépeau, V. Montouillout, A. Vimont, L. Mariey, T. Cseri, F. Maugé, Nature, Structure and Strength of the Acidic Sites of Amorphous Silica Alumina: An IR and NMR Study, The Journal of Physical Chemistry B. 110 (2006) 15172–15185. doi:10.1021/jp062252d.
[45] P. Kowalczyk, A. Deditius, W.P. Ela, M. Wiśniewski, P.A. Gauden, A.P. Terzyk, S. Furmaniak, J. Włoch, K. Kaneko, A.V. Neimark, Super-sieving effect in phenol adsorption from aqueous solutions on nanoporous carbon beads, Carbon. 135 (2018) 12–20. doi:10.1016/j.carbon.2018.03.063.

[46] C. Baerlocher, L.B. McCusker, D.H. Olson, Atlas of zeolite framework types, 6th rev. ed, Elsevier, page 141, Amsterdam, 2007.
[47] T. Martin, B. Lefevre, D. Brunel, A. Galarneau, F. Di Renzo, F. Fajula, P.F. Gobin, J.F. Quinson, G. Vigier, Dissipative water intrusion in hydrophobic MCM-41 type materials, Chemical Communications. 1 (2002) 24–25. doi:10.1039/b109081j.
[48] A. Cauvel, D. Brunel, F. Di Renzo, E. Garrone, B. Fubini, Hydrophobic and Hydrophilic Behavior of Micelle-Templated Mesoporous Silica, Langmuir. 13 (1997) 2773–2778. doi:10.1021/la962059i.
[49] A.T. Mohd Din, B.H. Hameed, A.L. Ahmad, Batch adsorption of phenol onto physiochemical-activated coconut shell, Journal of Hazardous Materials. 161 (2009) 1522–1529. doi:10.1016/j.jhazmat.2008.05.009.
[50] A. Popov, E. Kondratieva, L. Mariey, J.M. Goupil, J. El Fallah, J.-P. Gilson, A. Travert, F. Maugé, Bio-oil hydrodeoxygenation: Adsorption of phenolic compounds on sulfided (Co)Mo catalysts, Journal of Catalysis. 297 (2013) 176–186. doi:10.1016/j.jcat.2012.10.005.